Fracture behaviour of high-strength concrete at a wide range of loading rates

X.X. Zhang, G. Ruiz, R.C. Yu, M. Tarifa

Accepted Manuscript

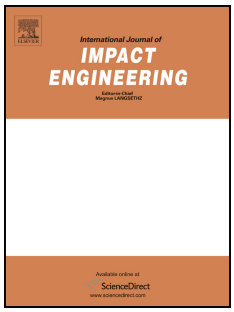

Title: Fracture behaviour of high-strength concrete at a wide range of loading rates

Authors: X.X. Zhang, G. Ruiz, R.C. Yu, M. Tarifa

PII: S0734-743X(09)00080-3

DOI: 10.1016/j.ijimpeng.2009.04.007

Reference: IE 1775

To appear in: *International Journal of Impact Engineering*

Received Date: 5 November 2008

Revised Date: 23 February 2009

Accepted Date: 22 April 2009

Please cite this article as: Zhang XX, Ruiz G, Yu RC, Tarifa M. Fracture behaviour of high-strength concrete at a wide range of loading rates, International Journal of Impact Engineering (2009), doi: 10.1016/j.ijimpeng.2009.04.007

Fracture behaviour of high-strength concrete at a wide range of loading rates

X.X. Zhang[1,2], G. Ruiz[2,*], R.C. Yu[2], M. Tarifa[2]

[1] *Harbin Engineering University, Harbin, China;*
[2] *Universidad de Castilla-La Mancha, Ciudad Real, Spain;*

Abstract

Three-point bending tests on notched beams of a high-strength concrete have been conducted using both a servo-hydraulic machine and a self-designed drop-weight impact device. The fracture energy and the peak load were measured over a wide range of loading point displacement rates, spanning eight orders of magnitude. Under low displacement rates, from 10^{-4} mm/s to 10 mm/s, the tests were performed with the servo-hydraulic machine; from 10^{2} mm/s to 10^{3} mm/s we used the drop-weight impact machine. The results show that the fracture energy and the peak load increase as the loading rate increases. Nevertheless, such a trend is relatively slight under low rates and can be attributed to viscous effects mainly originating from the presence of water in the pore structure. Under high rates the increases in the fracture energy and in the peak load are dramatic due to the effect of inertia.

Keywords: high-strength concrete; loading rates; drop-weight impact machine; fracture energy; dynamic increase factor

* Corresponding author: Tel.: +34-926295398; fax: +34-926295391.
Email address: Gonzalo.Ruiz@uclm.es

1. Introduction

Nowadays high strength concrete (HSC) is very often used in modern complicated structures of considerable height and span, such as skyscrapers, high towers and large bridges. These are more vulnerable to damages caused by earthquakes, wind and blast loading owing to the fact that HSC is more brittle than normal strength concrete (NSC). As a result, the dynamic fracture properties of HSC are more important than those of NSC with regard to safety assessment and the design of modern structures.

Over the past few decades, compared with the extensive research into the static fracture behaviour of HSC [1-16], much less information is available on its dynamic fracture behaviour [17-19]. Schuler et al. [18] measured the tensile strength and the fracture energy of high performance concrete (HPC) with spalling tests, and Mindess et al. [19] obtained dynamic mechanical properties of HSC and NSC using a drop weight impact machine. More detailed information about these results will be given later, in the section comparing our results with data already published. Nevertheless, experimental data on the rate sensitivity of the fracture properties of HSC are very scarce, as evidenced by Müeller in a recently published state-of-the-art report on constitutive modelling of HSC [17].

Thus, in order to get additional insights into the loading rate effect on the fracture properties of HSC, in this paper we present three-point bending tests conducted at a wide range of loading point displacement rates (for simplicity, it is substituted by loading rates), from 10^{-4} mm/s to 10^{3} mm/s, using both a hydraulic servo-controlled testing machine and a drop-weight impact instrument. The results show that both the fracture energy and the peak load increase with increases in loading rates. Under low loading rates, such tendency is slight, while under high loading rates it is significant. This paper also provides formulations

for the rate-dependency of the fracture energy and of the peak load, these will be helpful when simulating such rate dependency numerically.

This paper is structured as follows: the experimental procedure is given in section 2, in section 3 the results are presented and discussed. Finally, in section 4 some conclusions are drawn.

2. Experimental procedure

2.1 Material characterization

A single high strength concrete was used throughout the experiments, made with a Porphyry aggregate of 12 mm maximum size and ASTM type I cement, I 52.5R. Microsilica fume slurry and super plasticizer (Glenium ACE 325, B225) were used in the concrete composition. The mixing proportions by weight were 1:0.187:2.12:0.445:0.30:0.065 (cement: water: coarse aggregate: sand: microsilica fume slurry: super plasticizer).

There was a strict control of the specimen-making process, to minimize scattering in test results. All of the specimens were cast in steel molds, vibrated by a vibrating table, wrap-cured for 24 hours, demolded, and stored for 4 weeks in a moist chamber at 20℃ and 98% relative humidity until they were tested.

Compressive tests were conducted according to ASTM C39 and C469 (which are analogous to EN 12390-3 and EN 13412) on 75 mm×150 mm (diameter × height) cylinders. Brazilian tests were also carried out using cylinders of the same dimensions and following the procedures recommended by ASTM C496 (which is analogous to EN 12390-6). We made 8 cylinders, 4 for compression tests and 4 for splitting tests. Table 1 shows the

characteristic mechanical parameters of the concrete as determined in the various characterization and control tests. The classification of the concrete is C100/115 in reference to EN 206-1, and the mass density of the material is 2400 kg/m^3.

Table 1 Mechanical properties of the high-strength concrete

	f_c (MPa)	f_t (MPa)	E_c (GPa)
1	115.6	6.8	44.5
2	133.7	5.7	44.9
3	119.7	5.9	40.4
4	138.9	6.8	43.3
Mean	127.0	6.3	43.3
Std. Dev	11.1	0.6	2.0

2.2 Three-point bending fracture tests

In order to study the loading rate effect on the fracture behaviour of the HSC, three-point bending tests were conducted on notched beams over a wide loading rate range, from 10^{-4} mm/s to 10^3 mm/s. Two testing machines were adopted to carry out the tests, one was a hydraulic servo-controlled testing machine, the other was a self-designed drop-weight impact instrument.

The dimensions of the test beams were 100×100 mm^2 (B×D) in cross section, and 400 mm (L) in total length. The initial notch-depth ratio (a/D) was approximately 0.5, and the span (S) was fixed at 300 mm during the tests.

2.2.1 Tests under loading rates from 10^{-4} mm/s to 10^1 mm/s

In this low loading rate range, the tests were performed using the hydraulic servo-controlled testing machine as shown in Fig. 1.

In regard to the measuring method applied to obtain the fracture energy (G_F), we followed the procedures devised by Elices, Guinea and Planas [20-23]. G_F is obtained as:

$$G_F = \frac{W_{\exp} + W_{um}}{B(D - \mathrm{a})} \quad (1)$$

where W_{exp} is the area under the experimental load-displacement curve (P_{exp}-δ_{exp}), and W_{um} is the unmeasured energy that corresponds to the portion of the ligament that is still unbroken when we stop the test. We calculate this by assuming that the crack propagation obeys a cohesive model, which leads to a hyperbolic tail in the P-δ curve when the displacement is very large and the ligament is very short [22, 23]. Fig. 2 illustrates the process followed to obtain the complete fracture energy. δ_u and P_u correspond to the termination of the bending test. It should be noted that the kinetic energy of the specimen is very small and insignificant compared with the fracture energy in our tests. Moreover, the unmeasured energy is approximately 10% of that of the measured one.

In order to get the complete failure information from the specimen, the weight compensation technique was adopted during the test. i.e., springs were used to hold the specimen all the time as shown in Fig. 1. The beam rests on two rigid-steel cylinders laid on two supports permitting rotation out of the plane of the beam and rolling along the beam´s longitudinal axis with negligible friction. These supports roll on the upper surface of a very stiff beam fastened to the machine actuator. The load-point displacement is measured in relation to points over the supports on the upper surface of the beam.

Two LVDTs (linear variable differential transducers) fixed to the steel beam are used to measure the displacement between the loading rod and the steel beam. To load, a hydraulic servo-controlled test system was employed. The tests were performed in position-control. Three loading rates were applied during the test from quasi-static level (5.50×10^{-4}

mm/s) to rate dependent levels (5.50×10^{-1} mm/s and 1.74×10^{1} mm/s). Three specimens were tested at each loading rate.

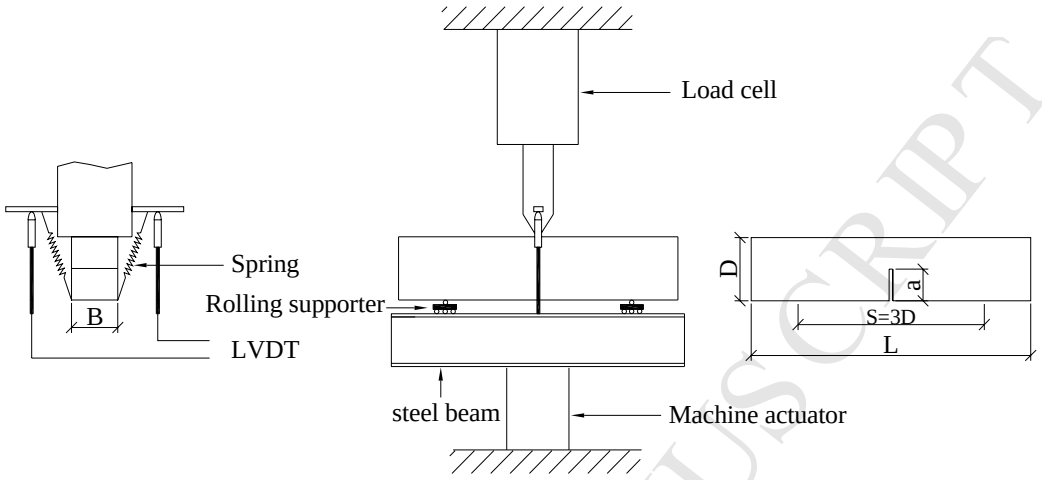

(a)

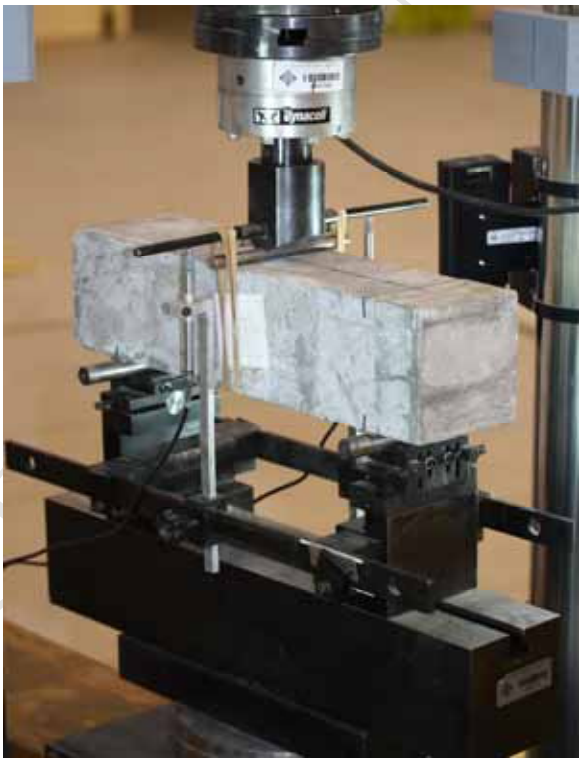

(b)

Fig. 1. (a) Schematic diagram and (b) photo of experimental set-up for three-point bending tests on beams.

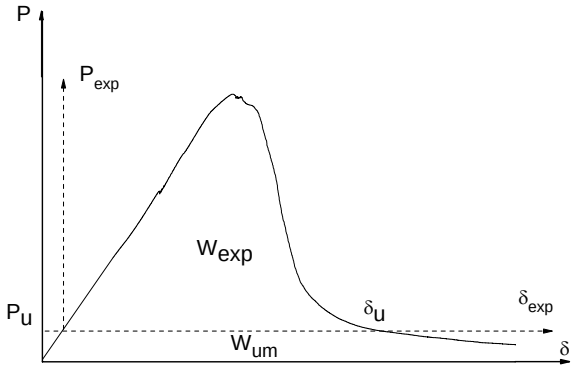

Fig. 2. Determination of the fracture energy.

2.2.2 Tests under loading rates from 10^2 mm/s to 10^3 mm/s

In this high loading rates range, all impact tests were conducted using the instrumented, drop-weight impact apparatus designed and constructed in the Laboratory of Materials and Structures of the Universidad de Castilla – La Mancha, as shown in Fig. 3. It has the capacity to drop a 316 kg mass from heights of up to 2.6 m, and can accommodate flexural specimens with spans of up to approximately 1.6 m. In this study, an impact hammer weighing 120.6 kg was used and three drop heights adopted were 40, 160 and 360 mm. Three specimens were tested at each drop height.

A detailed description of the instrument is given in reference [24]. The impact force between the hammer tup and the specimen is measured by a piezoelectric force sensor. In addition, the reaction force between the support and the specimen is determined by another two force sensors.

An accelerometer attached to the impact hammer was used to measure acceleration and displacement during the impact process. Assuming that the hammer displacement was essentially equal to the displacement of the specimen at the loading point, the velocity and the loading point displacement could be evaluated using the following equations [25].

The initial impact velocity of the hammer, $\dot{u}_h(0)$ is

$$\dot{u}_h(0) = \sqrt{2aH} \tag{2}$$

where a is the corrected gravitational acceleration ($9.71 \pm 0.14 m/s^2$), H stands for the hammer drop height. During the impact process, the velocity of the hammer can be obtained using Eq. 3.

$$\dot{u}_h(t) = \dot{u}_h(0) + \int_0^t \ddot{u}_h(t)dt \tag{3}$$

where $\ddot{u}_h(t)$ is the acceleration recorded by the accelerometer attached to the hammer. Then, the displacement of the hammer, $u_h(t)$ and also the loading point displacement of the specimen is calculated by Eq. 4.

$$u_h(t) = \int_0^t \left[\dot{u}_h(0) + \int_0^t \ddot{u}_h(t)dt \right] dt \tag{4}$$

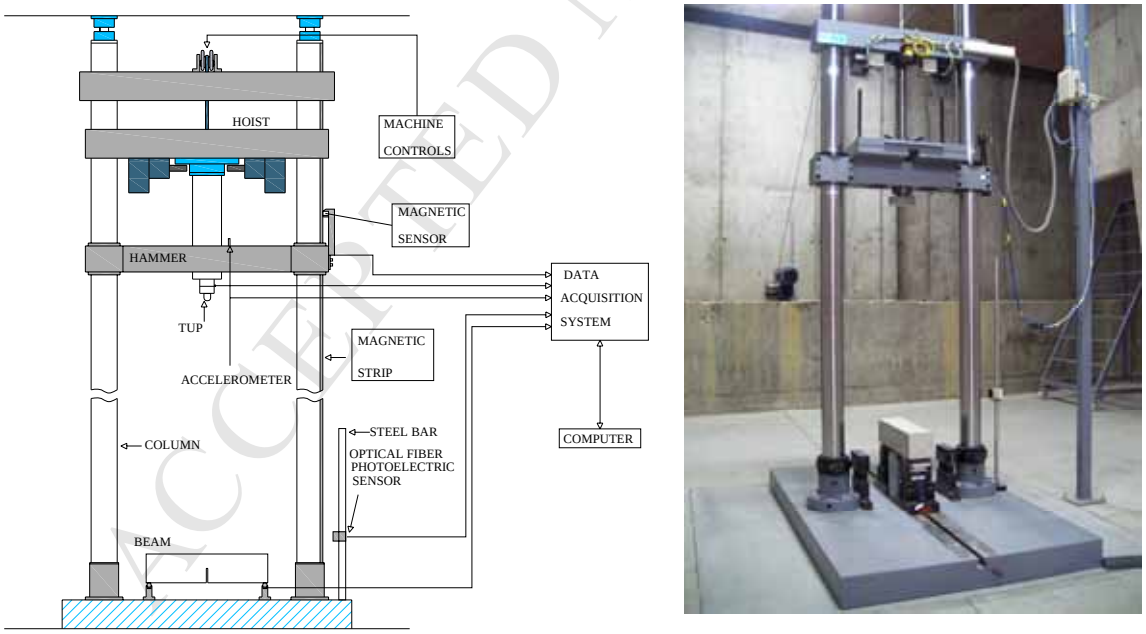

(a) (b)

Fig. 3. (a) Schematic diagram and (b) photo of the drop-weight impact machine.

In reference [24], for measuring the loading point displacement of the specimen during impact process, three accelerometers were mounted along the length of the beam. Thus, the displacement of each location of the accelerometer attached can be obtained by double integration of the acceleration and, then, the loading point displacement can be determined by linear extrapolation.

It is very easy to damage the cables and accelerometers when using a heavy hammer during the tests, thus, in this work we used an accelerometer bonded on the hammer to get the loading point displacement instead assuming that the loading point displacement of the specimen is identical to that of the hammer.

In order to verify this assumption, we performed tests using both methods to capture the loading point displacement. For protecting cables and accelerometers, steel yokes were used to fix the specimen, so that the specimen can not bound from the support, the hammer drop height was 100 mm. Fig. 4 shows the comparison of results using the two methods to measure the loading point displacement. It is clear that their tendency versus time and the order in magnitude are the same. When the specimen is broken, the loss of contact between the hammer and the specimen makes that the differences between experimental results obtained by the two methods are bigger. So, we think that the assumption that the loading point displacement of the specimen is identical to that of the hammer is reasonable.

under dynamic loading conditions, there is neither a standard nor any generally accepted procedure for measuring fracture energy. In this case, it is not that clear that the fracture energy is not fully measured, since the ligament in the dynamic tests ends up completely broken. So, we decide to give the measured value, not accounting for any type of unmeasured energy. The measured energy is calculated by the area under the reaction

force-displacement (load-displacement) curves, where the reaction force is evaluated by adding the values from both support data points [24, 26].

Furthermore, we did not use any kind of damping materials during the tests, nor did we observe any compressive damage in the impact area.

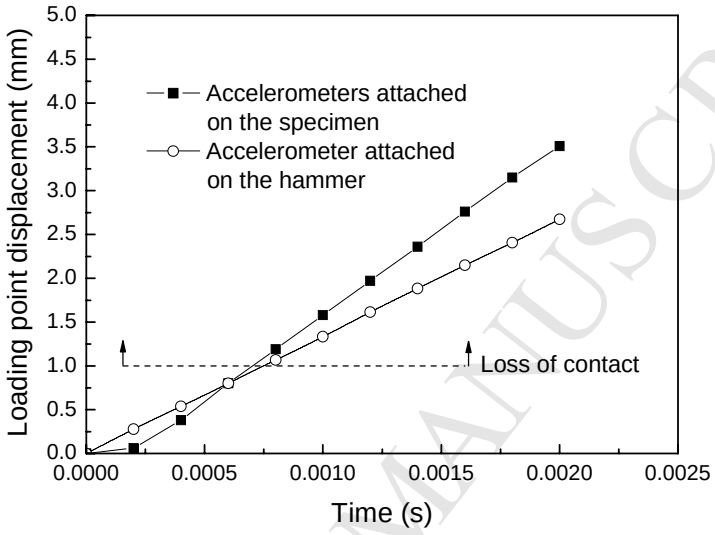

Fig. 4 Comparison of the loading point displacement

3. Results and discussion

3.1 Experimental results

Fig. 5 shows the comparison of the typical load-displacement curves at different loading rates. It is clear that the peak load increases in line with increases in loading rates. However, the stiffness of the beam does not show a similar tendency, which is due to the sensitivity of the elastic flexibility of the beam to the boundary conditions during the application of the concentrated load [27].

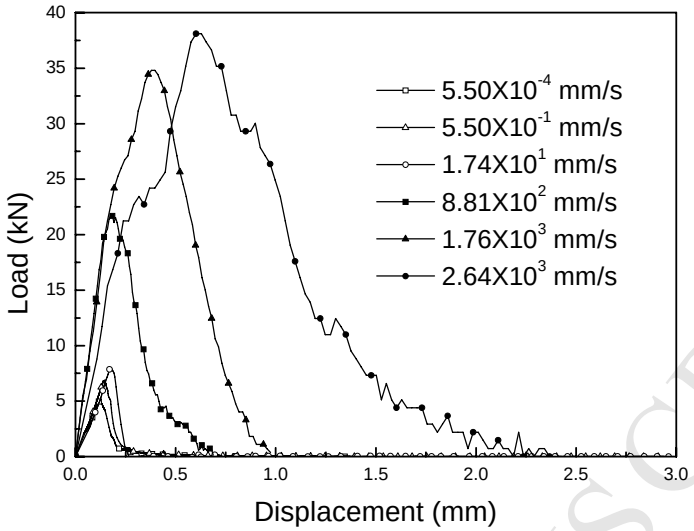

Fig. 5. Load-displacement curves at different loading rates.

Table 2 provides detailed information about the experimental results. The data in the parenthesis are the standard deviation. The dynamic increase factor (*DIF*), is defined by the ratios of peak load (P_{max}) and of the fracture energy to their corresponding quasi-static values. Here, the lowest loading rate ($\dot{\delta} = 5.50 \times 10^{-4}$ mm/s) is taken as the quasi-static loading condition. *H* stands for the drop height of the hammer under impact loading conditions.

Table 2 Experimental results at different loading rates.

Testing machine	*H* (mm)	$\dot{\delta}$ (mm/s)	P_{max} (kN)	*DIF* for P_{max}	W_F (N/m)	*DIF* for W_F
Hydraulic servo-controlled device	-	5.50×10^{-4}	5.33 (0.33)	1	148 (9)	1
	-	5.50×10^{-1}	7.20 (0.30)	1.35	205 (12)	1.39
	-	1.74×10^{1}	8.22 (0.37)	1.54	226 (19)	1.53
Drop-weight impact instrument	40	8.81×10^{2}	23.87 (3.10)	4.48	1205 (24)	8.14
	160	1.76×10^{3}	34.34 (2.73)	6.44	3968 (653)	26.81
	360	2.64×10^{3}	38.07 (7.65)	7.14	5658 (885)	38.23

Fig. 6 shows the loading rate effect on the fracture energy. It is clear that the fracture energy increases with increases in loading rates, it should also be noted that beyond a certain threshold (7.04×10^2 mm/s) the rate effect becomes more pronounced and a significant increase is observed. A prediction equation for the loading rate effect on the fracture energy is derived from the test data.

$$\begin{cases} G_F = G_F^S(1+m\dot{\delta}^r) = 147.5(1+0.34\dot{\delta}^{0.17})\,[\text{N/m}], & \text{for } \dot{\delta} < 7.04\times10^2\,\text{mm/s} \\ G_F = -26171.16 + 9296.4 log\dot{\delta}\,[\text{N/m}], & \text{for } \dot{\delta} \geq 7.04\times10^2\,\text{mm/s} \end{cases} \quad (5)$$

where G_F^S is the static fracture energy. Exponents *m* and *r* are adjusting parameters, $\dot{\delta}$ is the loading rate given in mm/s. Eq. 5 can be used to efficiently predict the loading rate effect on the fracture energy and could also be helpful when performing numerical simulations. It is worth noting that 147.5 N/m obtained by fitting the experimental data is the static value of the fracture energy, and that this could only be obtained by a strictly static test [28].

Under low loading rates, those less than the threshold, the rate effect is slight, and it can be attributed to viscous effects mainly originated by the presence of free water in voids and porous structures. The fact that dry concrete exhibits very little rate sensitivity, except at very high strain rates, provides further justification for our explanation of this tendency [29].

However, under impact loading rates, greater than the threshold, the rate effect is remarkable due to the inertia effect [30-32]. Furthermore, the high increase in the fracture energy is caused by many micro-cracks that develop under impact loading [30, 33, 34]. Namely, at high loading rates the mechanism of failure is characterized by the propagation

of many micro-cracks at the same time, these micro-cracks do not have sufficient time to search for paths of minimum energy or lowest resistance. Thus, they are forced to propagate along the shortest path with higher resistances, this leads us straight to the conclusion that the fracture energy should increase as a function of the loading rate.

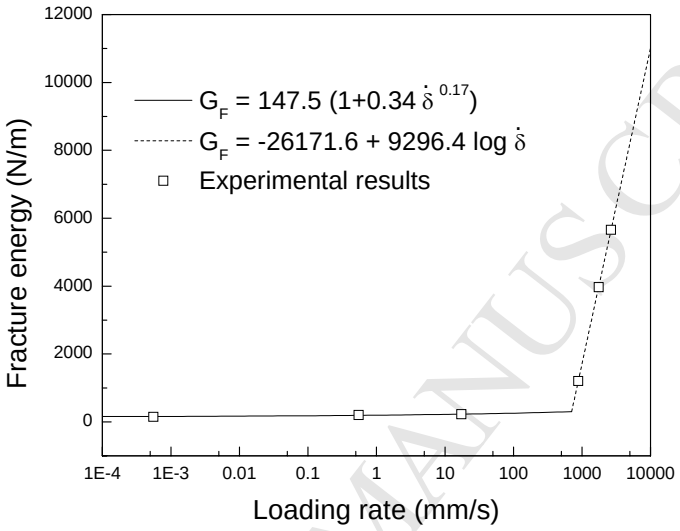

Fig. 6. Loading-rate dependence of the fracture energy

Fig. 7 shows the loading rate effect on the peak load, the trend is similar to that of the fracture energy. i.e., under low loading rates, the tendency is moderate, while under high loading rates it is dramatic. The maximum *DIF* for the peak load is 7.14, compared with 38.23 for the fracture energy. It could be that the fracture energy is more sensitive to micro-cracks than the peak load under high loading rates. This also makes it possible to use only one exponential function to describe the behavior of peak load versus loading rates. Fig. 6 presents the function as well, namely,

$$P_{\max} = P_{\max}^{S}(1 + k\dot{\delta}^{n}) = 5.88(1 + 0.10\dot{\delta}^{0.51})[\text{kN}], \text{ for } \dot{\delta} \text{ in mm/s} \qquad (6)$$

where $P_{\max}^{S}$ is the static peak load, exponents k and n are adjusting parameters. It is noteworthy that the fitting also gives the static value of the peak load, 5.88 kN.

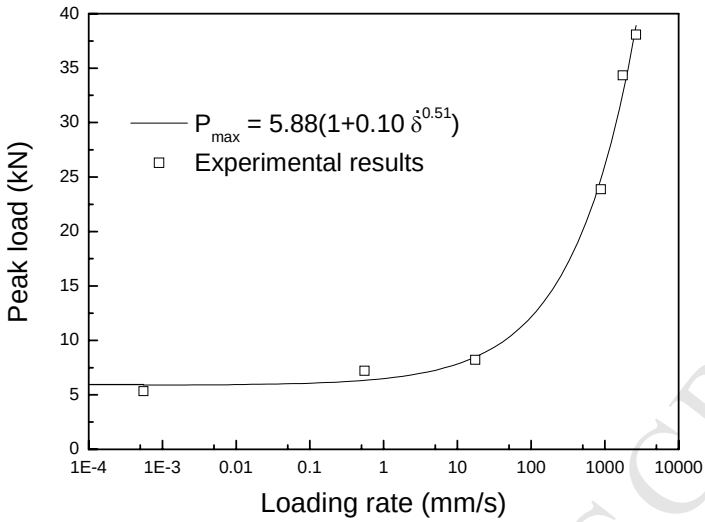

Fig. 7. Loading rate dependence of the peak load

3.2 Comparison with data already published

As mentioned before, compared with the extensive research into the quasi-static fracture behaviour of HSC, much less information is available on its rate-sensitivity behaviour. Table 3 provides a comparison of some impact experimental results from Mindess et al. [19] and the results presented in this paper. The definition of high-strength concrete continues to change as advances in concrete technology make it easier to achieve increasingly higher strengths using conventional construction practices, thus, the compressive strength of the HSC in the paper is around two times bigger than that used in reference [19].

From this table it is clear that the trend of the loading rate effect on the mechanical properties of both high strength concretes is similar, however a big difference is found in the *DIF* for the peak load. It could be that this is more relevant due to the differences in the span/width ratio during the tests. In general, the weight of the hammer, the impact energy

and the dimensions of the beams do affect the experimental results. Nevertheless, the results from different drop-weight impact machines are comparable.

Schuler et al. [18] measured the tensile strength and the fracture energy of High Performance Concrete (HPC) at high strain rates between 10 /s and 100 /s with spalling tests. A *DIF* of 3 was observed at a crack opening velocity of 1.7 m/s for the fracture energy. This does not concur with the experimental results obtained by drop-weight impact tests, which can partly be attributed to the inconsistency among the methods of loading and associated errors.

Furthermore, under low loading rates, the rate sensitivity of the fracture energy is slight compared with the fracture energy variation at high loading rates. This leads some authors to conclude that the fracture energy is constant and rate independent at low loading rates [35-37].

Table 3 Comparison of experimental results

	Experimental results from Mindess et al. [19]	Experimental results in this paper
Compressive strength (MPa)	62	127
Dimensions of the beam (width × depth × length) (mm)	100×125×1400	100×100×400
Span (mm)	960	300
Drop height of the hammer (mm)	150	160
Weight of the hammer (kg)	345	120.6
DIF for the peak load	2.96	6.44
DIF for the fracture energy	21.38	26.74

4. Conclusions

The fracture behaviour of a high strength concrete under dynamic loading conditions was investigated in this study. The loading rates varied considerably from a quasi-static

level to a dynamic level, the order of magnitude changed from 10^{-4} mm/s to 10^{3} mm/s. As a result of the study, the following conclusions can be drawn.

(1) The fracture energy is sensitive to the loading rate. Under low loading rates, below 7.04×10^{2} mm/s, the rate effect is slight, and can be attributed to viscous effects mainly originated by the presence of free water in voids and porous structures. However, the rate effect is pronounced when the loading rate goes beyond the threshold of 7.04×10^{2} mm/s.

(2) The peak load and the fracture energy both increase with increases in loading rates, however, under high loading rates the effect on the fracture energy is even more pronounced than that on the peak load.

(3) Finally, two prediction-equations for the rate sensitivity of the fracture energy and the peak load are proposed. These formulas are helpful in numerical simulations that evaluate the rate dependence of fracture behaviour.

Acknowledgements

Funding from the *Ministerio de Ciencia e Innovación*, Spain, under grant MAT2006-09105 and from the *Consejería de Educación y Ciencia*, JCCM, Spain, under grant PAI08-0196, is gratefully acknowledged.

References

[1] Yan A, Wu KR, Zhang D, Yao W. Effect of fracture path on the fracture energy of high-strength concrete. Cement and Concrete Research 2001; 31: 1601-1606.
[2] Einsfeld RA, Velasco MSL. Fracture parameters for high-performance concrete. Cement and Concrete Research 2006; 36: 576-583.
[3] Zhang J, Liu Q, Wang L. Effect of coarse aggregate size on relationship between stress and crack opening in normal and high strength concretes. Journal of Materials Science and Technology 2005; 21: 691-700.
[4] Sagar RV, Dinesh SV, Santosh AC. Fracture energy of normal and hsc beams. Indian Concrete Journal 2005; 79: 37-42.
[5] Bharatkumar BH, Raghuprasad BK, Ramachandramurthy DS, Narayanan R, Gopalakrishnan S. Effect of fly ash and slag on the fracture characteristics of high performance concrete. Materials and Structures/Materiaux et Constructions 2005; 38: 63-72.
[6] Chen B, Liu J. Effect of aggregate on the fracture behavior of high strength concrete. Construction and Building Materials 2004; 18: 585-590.
[7] Appa Rao G, Raghu Prasad BK. Strength and fracture toughness of interface in high strength concrete. Journal of Structural Engineering (Madras) 2003; 30: 153-161.
[8] Wittmann FH. Crack formation and fracture energy of normal and high strength concrete. Sadhana - Academy Proceedings in Engineering Sciences 2002; 27: 413-423.
[9] Rao GA, Prasad BKR. Fracture energy and softening behavior of high-strength concrete. Cement and Concrete Research 2002; 32: 247-252.
[10] Wu KR, Chen B, Yao W, Zhang D. Effect of coarse aggregate type on mechanical properties of high-performance concrete. Cement and Concrete Research 2001; 31: 1421-1425.
[11] Dong Z, Keru W. Fracture properties of high-strength concrete. Journal of Materials in Civil Engineering 2001; 13: 86-88.
[12] Darwin D, Barham S, Kozul R, Luan S. Fracture energy of high-strength concrete. ACI Materials Journal 2001; 98: 410-417.
[13] Li Q, Ansari F. High-strength concrete in uniaxial tension. ACI Structural Journal 2000; 97: 49-57.
[14] Gettu R, Garcia-Álvarez VO, Aguado A. Effect of aging on the fracture characteristics and brittleness of a high-strength concrete. Cement and Concrete Research 1998; 28: 349-355.
[15] Marzouk H, Chen ZW. Fracture energy and tension properties of high-strength concrete. Journal of Materials in Civil Engineering 1995; 7: 108-116.
[16] Gettu R, Bazant ZP, Karr ME. Fracture properties and brittleness of high-strength concrete. ACI Materials Journal 1990; 87: 608-618.
[17] Müeller H. Constitutive modelling of high strength / high performance concrete - state of the art report. CEB FIP Bulletin 42, 2008.
[18] Schuler H, Hansson H. Fracture behaviour of high performance concrete (hpc) investigated with a hopkinson-bar. Journal De Physique. IV : JP. Dijon, 2006: p. 1145-1151.
[19] Mindess S, Banthia N, Yan C. Fracture toughness of concrete under impact loading. Cement and Concrete Research 1987; 17: 231-241.

[20] Guinea GV, Planas J, Elices M. Measurement of the fracture energy using 3-point bend tests .1. Influence of experimental procedures. Materials and Structures 1992; 25: 212-218.
[21] Planas J, Elices M, Guinea GV. Measurement of the fracture energy using 3-point bend tests .2. Influence of bulk energy-dissipation. Materials and Structures 1992; 25: 305-312.
[22] Elices M, Guinea GV, Planas J. Measurement of the fracture energy using 3-point bend tests .3. Influence of cutting the p-delta tail. Materials and Structures 1992; 25: 327-334.
[23] Elices M, Guinea GV, Planas J. On the measurement of concrete fracture energy using three-point bend tests. Materials and Structures 1997; 30: 375-376.
[24] Zhang XX, Ruiz G, Yu RC. A new drop-weight impact machine for studying fracture processes in structural concrete. Strain 2008; (in press).
[25] Sukontasukkul P, Nimityongskul P, Mindess S. Effect of loading rate on damage of concrete. Cement and Concrete Research 2004; 34: 2127-2134.
[26] Banthia N, Mindess S, Bentur A, Pigeon M. Impact testing of concrete using a drop-weight impact machine. Experimental Mechanics 1989; 29: 63-69.
[27] Planas J, Guinea GV, Elices M. Stiffness associated with quasi-concentrated loads. Materiaux et constructions 1994; 27: 311-318.
[28] Ruiz G, Zhang XX, Del Viso JR, Yu RC, Carmona JR. Influence of the loading rate on the measurement of the fracture energy of a high strength concrete. Anales de Mecánica de la Fractura 2008; 25: 793-798.
[29] Mindess S, Young JF, Darwin D. Concrete. United States of America: Prentice Hall, Pearson Education, Inc. United States of America, 2003.
[30] Brara A, Klepaczko JR. Fracture energy of concrete at high loading rates in tension. International Journal of Impact Engineering 2007; 34: 424-435.
[31] Weerheijm J, Van Doormaal JCAM. Tensile failure of concrete at high loading rates: New test data on strength and fracture energy from instrumented spalling tests. International Journal of Impact Engineering 2007; 34: 609-626.
[32] Rossi P, Toutlemonde F. Effect of loading rate on the tensile behaviour of concrete : Description of the physical mechanisms. Materials and Structures/Materiaux et Constructions 1996; 29: 116-118.
[33] Bischoff PH, Perry SH. Compressive behaviour of concrete at high strain rates. Materiaux et constructions 1991; 24: 425-450.
[34] Vegt I, Breugel VK, Weerheijm J. Failure mechanisms of conrete under impact loading. In: Carpinteri A, Gambarova P, Ferro G, Plizzari G (eds) Fracture Mechanics of Concrete and Concrete Structures. Italy, Catania: Taylor & Francis Group, 2007: p. 579-587.
[35] Birkimer D, Lindemann R. Dynamic tensile test of concrete materials. ACI Materials Journal 1971; 68: 47-49.
[36] Weerheijm J. Concrete under impact tensile loading and lateral compression, vol. PhD Thesis: PhD Thesis, Delft University of Technology, 1992.
[37] Schuler H, Mayrhofer C, Thoma K. Spall experiments for the measurement of the tensile strength and fracture energy of concrete at high strain rates. International Journal of Impact Engineering 2006; 32: 1635-1650.